Evidence of Alfvenic Poynting Flux as the Primary Driver of Auroral Motion During a Geomagnetic Substorm

Tian, S.
Colpits, C.
Wygant, J. R.
Cattell, Cynthia A.
Ferradas, C. P.
Larsen, Brian Arthur
Reeves, Edmond Geoffrey David
Donovan, E.
Kletzing, C. A.

To be published in: Journal of Geophysical Research: Space Physics

DOI to publisher's version: 10.1029/2020JA029019

Evidence of Alfvenic Poynting flux as the primary driver of auroral motion during a geomagnetic substorm

S. Tian[1], C. A. Colpitts[1], J. R. Wygant[1], C. A. Cattell[1], C. P. Ferradas[2], A. B. Igl[1,4], B. A. Larsen[2], G. D. Reeves[2], and E. F. Donovan[3]

[1]School of Physics and Astronomy, University of Minnesota, Minneapolis, Minnesota, United States
[2]Los Alamos National Laboratory, Los Alamos, New Mexico, United States
[3]Department of Physics and Astronomy, University of Calgary, Calgary, Alberta, Canada
[4]Department of Physics and Astronomy, Louisiana State University, Baton Rouge, Louisiana, United States

Key Points:

- We report the one-to-one correlation between a discrete arc and enhanced Poynting flux
- Alfvenic Poynting flux directly powers auroral acceleration
- Dipolarization may be related to Alfven wave generation

Corresponding author: Sheng Tian, tianx138@umn.edu

Abstract

Geomagnetic substorms are major energy transfer events where energy stored in the Earths magnetotail is released into the ionosphere. Substorm phenomena, including auroral activities, earthward Poynting flux, magnetic field dipolarization, etc, have been extensively studied. However, the complex interplay among them is not fully understood. In a fortuitous event on June 07, 2013, the twin Van Allen Probes (separated by 0.4 hour in local time) observed bursts of earthward Alfvenic Poynting flux in the vicinity of the plasma sheet boundary layer (PSBL). The Poynting flux bursts correlate with enhancements of auroral brightness around the footpoints of both spacecraft. This indicates a temporal and spatial correlation between the auroral brightening and Poynting flux bursts, and that the auroral motion is directly linked to the perpendicular expansion of the Alfven wave. These observations suggest that the Alfvenic Poynting flux is a primary driver for the auroral electron acceleration. Around the time of auroral brightening, a dipolarization was seen to propagate more than 4 hours in local time during a 20 min period. The azimuthal phase speed of this dipolarization (2 deg/min) is too small to explain the azimuthal motion of the aurora (13.6 deg/min), but the dipolarization could be related to the generation of the Alfvenic Poynting flux through phase mixing at strong density gradients like those in the PSBL.

1 Introduction

Auroral substorms involve the sudden brightening and spatial expansion of auroral activity in the nightside ionosphere (Akasofu, 1964). Low-altitude in-situ observations have shown that the auroral activity is directly connected to the magnetic flux tubes of the upward current region (Chapter 4 in Paschmann et al., 2003, and references therein). Within these flux tubes, electrons are accelerated toward the ionosphere in the auroral acceleration region (about 2-4 Re geocentric distances). This occurs primarily through two major mechanisms: quasi-static potential drops (McFadden et al., 1999) and kinetic Alfven waves (Chaston et al., 2004). Although strong wave-particle interaction occurs in the auroral acceleration region, it is clear that the free-energy source for the energy conversion lies at higher altitude.

In-situ measurements in the magnetotail have shown that the auroral substorm is one aspect of the more general concept of geomagnetic substorm, which involves sudden release of the magnetic energy stored in the tail. There are a variety of interrelated phenomena resulting from the energy release that can be observed including magnetic field dipolarization (Runov et al., 2009), enhanced earthward Poynting flux (Ergun et al., 2015), and plasma flow channels (Angelopoulos et al., 1992). As the magnetic flux tubes connect the ionosphere to the plasma sheet and its boundary layer in the magnetotail, the coupling between the ionosphere and magnetotail during substorms has been a focus of research for decades.

Conjunction studies between high-altitude in-situ observations and ionospheric or low-altitude measurements have been a powerful tool to study the coupling between the auroral ionosphere and magnetotail. The Polar spacecraft routinely sampled the plasma sheet boundary layer (PSBL) at 4-6 Re, providing in-situ measurements in magnetic conjunction with the auroral zone. Polar conjunctions have highlighted enhanced earthward Poynting fluxes as an important energy source for the auroral acceleration (Keiling et al., 2003). The Poynting fluxes are carried in the form of Alfven waves and kinetic Alfven waves (Wygant et al., 2000, 2002). However, one-to-one correlation has not been reported due to limited spatial and temporal resolution of auroral measurements. In this study, with improved auroral measurements in conjunction with two azimuthally separated Van Allen Probes, we show a spatial and temporal correlation holds between Alfvenic Poynting flux bursts and the brightening of a discrete arc in motion.

The azimuthal motion of the aurora has previously been linked to the azimuthal propagation of dipolarizations (Angelopoulos et al., 2008; Ogasawara et al., 2011). The azimuthal phase speed of the auroral motion is typically on the order of 10-20 deg/min (Paschmann et al., 2003; Angelopoulos et al., 2008; Ogasawara et al., 2011). This speed corresponds to dipolarizations propagate at 150 km/s at geosynchronous orbit along the azimuthal direction. Although such "fast" dipolarizations are reported in many events (Angelopoulos et al., 2008; Ogasawara et al., 2011), statistical studies show that the typical value of the azimuthal phase speed of the dipolarizations is only 30-50 km/s (Nagai, 1982; Ohtani et al., 2018) at geosynchronous orbit. In Section 4, we discuss the nature of the "fast" dipolarizations, the apparent speed difference between the "fast" and "slow" dipolarizations, and their relation to the auroral motion and Alfvenic Poynting flux.

In the rest of the paper, we present a case study of a substorm where the Alfvenic Poynting flux is shown to be the driver of auroral motion. The instrumentation used is outlined in Section 2. The observations are presented in Section 3. The results are discussed in Section 4. In Section 5, we offer some conclusions based on these results.

2 Instrumentation

Although the orbits of the Van Allen Probes (RBSP) tend to maximize time around the equatorial plane, they can be in conjunction with the auroral zone for many hours per orbit due to the wobble of the earths dipole. Therefore, these probes can be surprisingly suitable to investigations of auroral physics. The spacecraft provide DC measurements of the electric and magnetic fields with the EFW (Wygant et al., 2013) and EMFISIS (Kletzing et al., 2013) instruments. The DC electric (magnetic) field data are available at 16 (32) samples/sec. Magnetic field data are thus down sampled to 16 samples/sec to calculate the 3D Poynting flux. Within the calculation, the DC electric field along the spin axis is not well measured and thus is calculated using the $\vec{E} \cdot \vec{B} = 0$ assumption. Note that for calculating the parallel Poynting flux, the spin axis electric fields are not important because the spin axis is primarily along the background magnetic field during nightside events like the one in this paper. In addition, the HOPE (Funsten et al., 2013; Spence et al., 2013) instrument onboard RBSP provides measurements of the electrons and H+, He+, O+ from several eV to 50 keV per charge at an alternating electron ion ∼11 cadence, ∼22 sec between subsequent ion measurements). The data are collected in 5 look directions, 16 spin angles, and 72 log-spaced energy bins. In conjunction with the RBSP spacecraft, the THEMIS all-sky imager (ASI) (Mende et al., 2008) at Pinawa, Manitoba, CA (PINA) records auroral images every 3 sec at a typical spatial resolution of 1 deg. This high temporal and spatial resolution enables us to resolve discrete arcs and their motions.

3 Observations

Figure 1a shows a substorm that occurred from around 04:47 to 04:57 UT on June 07, 2013. Panel a shows the Dst (black) and AE (red) indices from 04:30 to 05:30 UT, with Dst at ~ -80 nT and AE above 1000 nT around 04:50 UT. This occurs in the early recovery phase of a moderate geomagnetic storm. Panel b shows the detrended tilt angle of the measured magnetic field as a function of UT and MLT, with positive (more dipolar) angles showing as red, as measured on the GOES-13 and -15 and RBSP-A and -B spacecraft. During the substorm, a dipolarization was seen from midnight to at least 20 MLT. The dipolarization is characterized by the sudden increase of the detrended tilt angle of the measured magnetic field $B_{x,y,z}$. The original tilt angle $\alpha = \arcsin B_z/|B|$ is first detrended using the T89 model (N. A. Tsyganenko, 1989) and then smoothed over a 60 min window to remove the remaining offset. The detrended tilt angle is color-coded along the spacecraft tracks in panel b and plotted

over a shorter time range in panel c and d. In panel b, a linear fit on the times and MLTs of the major ramps of increasing tilt angle (where blue turns to red) determines the angular speed as 2 deg/min, which scales to ∼20 km/s at 5 Re (arrow in panel e). Panels c and d zoom in to a shorter time range and show the tilt angle (red) and density (gray and black) observed on RBSP-A (panel c) and -B (panel d). At both spacecraft, the dipolarization was accompanied by density fluctuations. The dipolarization and density fluctuation are clearly time-lagged, with peaks on RBSP-B occurring ∼2 min after the peaks are observed on RBSP-A. The density is consistently determined by the particle instrument (gray, low resolution) and by the spacecraft potential (black, high resolution). The time lag between the density structure is 147.2 sec, determined by cross-correlating the density from the spacecraft potential. Based on this time lag, the local angular speed of the density structure is 2.4 deg/min around 22 MLT, which is consistent with the global value (2 deg/min) of the dipolarization speed calculated from the data shown in panel b. In addition, the MHD plasma velocity along the azimuthal direction was calculated to be 20(26) km/s westward at RBSP-A(-B). The speed match along the azimuthal direction among the dipolarization, density structure, and plasma motion suggests that the dipolarization propagated along with plasma motion. This speed will be further discussed and compared to previous studies (Angelopoulos et al., 2008; Ogasawara et al., 2011; Nagai, 1982; Ohtani et al., 2018) in Section 4. RBSP-A and -B were in the PSBL before around 05:05 UT, when both spacecraft saw increases in the electron temperature from several keV to several 10s of keV and electron density from several 0.1s to above 1 cm^{-3} (not shown). These are typical features when a spacecraft enters the central plasma sheet from PSBL.

Figure 2 shows the Poynting flux (panel 4) and the frequency spectra of the parallel component of the Poynting flux (panel 5), calculated from the wave electric (panel 2) and magnetic (panel 3) fields observed on RBSP-A (Figure 2a) and -B (Figure 2b). The electric field data along the spin-axis is calculated using the perpendicular components based on the $\vec{E} \cdot \vec{B} = 0$ assumption. This calculation does not affect the parallel Poynting flux much, representing a 10% correction in this event, because the spin-axis was approximately along the background magnetic field during the substorm. The Poynting flux was calculated using a Morlet wavelet in the frequency range of 4 mHz to 10 Hz, or from 0.1 sec to 250 sec in terms of wave period. Panels a-4 and b-4 show that the Poynting fluxes were predominantly earthward (positive parallel Poynting flux, red curve) at both spacecraft, >10 mW/m^2 after normalized to 100 km altitude to account for the converging flux tube. Panels a-5 and b-5 show that the main power is between 0.01 to 0.1 Hz. The E/B ratio in this frequency range was comparable to the local Alfven speed (panels a-8 and b-8), suggesting that the earthward Poynting flux was due to a shear Alfven wave (shear mode as no significant $|B|$ is seen). The power spectra of the magnetic field follows the Kolmogorov law (panels a-7 and b-7), suggesting a turbulent environment which may lead to cascades from shear Alfven waves to smaller scale waves like kinetic Alfven waves.

Figure 3 shows several snapshots of auroral activity observed every 15 seconds from 04:55 to 04:56 UT (panels a-e), and at 04:58 UT (panel f) at the PINA THEMIS All-Sky Imager (the Movie S1 of the supporting information includes all images observed, every 3 seconds, during this time interval). Aurora first brightened around 04:55 UT, then traveled westward (panels a and b), expanded poleward (panels b to d), and finally faded (panels e and f). Because the in-situ measurements are primarily azimuthal, we only focus on the westward motion of the aurora. Figure 4 shows four snapshots capturing this east/west motion (panels a-d), as well as an EWOgram (photon count within an MLat bin as a function of MLon and time) of the aurora within MLat of 63-64.5 deg to further illustrate and quantify this westward motion. The time of each of the snapshots is indicated by red arrows to the left of this panel, the location of the brightest aurora shown by red boxes, and the line with the best fit to these boxes is over plotted in red as well. The slope of this line gives us the westward motion of

the aurora, determined to be 13.6 deg/min through this linear fit. This speed scales to ∼120 km/s at 5 Re for comparisons to the in-situ measurements. This speed is ∼6 times larger than the calculated speed of the dipolarization. The relationship between the dipolarization and aurora, which were co-observed during the substorm, will be further discussed in Section 4.

This observed auroral activity can be directly compared to in-situ observations of Alfvenic Poynting flux in the plasma sheet boundary layer along the same magnetic field lines. Figure 5 shows the Poynting flux observed on RBSP and the auroral brightness around the ionospheric footpoint of the satellites. The footpoint determined from the Tsyganenko models, including T89, T96, T01, and T04 (N. A. Tsyganenko, 1989; N. Tsyganenko, 1996; N. A. Tsyganenko, 2002; N. A. Tsyganenko & Sitnov, 2005), is consistent in MLon but uncertain in MLat. Because the mapping is accurate in MLon, the KEOgram (photon count within an MLon bin as a function of MLat and time) is used to track the auroral motion, and is shown in panels a-1 and b-1. Also in these panels, the MLat footpoint location given by the four models is shown and can be seen to vary from ∼61.8 to 65.9 degrees. To eliminate this uncertainty, two methods are used to pin down the MLat of the footpoint. First, we compare the measured in-situ magnetic field to the models. The T01 model is found to provide the best prediction. Secondly, we cross-correlate the auroral brightness at all possible MLat to the Poynting flux. The results of this cross-correlation are shown as a function of MLat in panels a-2 and b-2, with the peak of the correlation and the full width-half max (FWHM) shown as well. At both spacecraft, the cross-correlation peaks around the T01 MLat within the FWHM error bar. Therefore, the T01 model is used for mapping in this event. Panels a-3 and b-3 plot the auroral brightness at the T01 footpoint against the parallel Poynting flux. The comparison shows a clear correlation between the two quantities at each satellite. More importantly, the fact that this correlation holds at two spacecraft separated along the direction of the auroral westward motion suggests a dynamical picture where the auroral motion is directly linked to the perpendicular expansion of the Alfvenic Poynting flux. The spatial and temporal correlation provide strong evidence that the Poynting flux, transmitting significant electromagnetic energy earthward, is an important (if not the only) energy source that powers the auroral acceleration.

4 Discussion

We have used a close magnetic conjunction between the Van Allen Probes and the PINA ASI during a geomagnetic substorm on June 07, 2013, to investigate the coupling between the auroral ionosphere and the near-Earth (5-6 Re) plasma sheet and its boundary layer . Significant bursts of earthward Alfvenic Poynting flux (>50 mW/m^2 when normalized to 100 km altitude) were observed during the brightening and expansion of a discrete auroral arc. Although previous studies have highlighted the correlation between Poynting flux and aurora (Wygant et al., 2000; Keiling et al., 2003), this is the first time this correlation has been resolved down to auroral structures like a discrete arc, which can now be spatially resolved due to the improved auroral observations. In addition, the fact that both RBSP-A and -B were in conjunction with the discrete arc enables us to study the relation between the Poynting flux and aurora in a dynamical picture. We find that the Poynting flux correlated with the auroral brightness at the footpoint of spacecraft at both Van Allen Probes. The correlation at each footpoint shows that the auroral activity was driven by the Alfvenic Poynting flux, i.e., the electromagnetic energy transmitted in the form of Alfven waves along the magnetic field line. The correlation at both footpoints shows that the auroral motion was directly linked to the perpendicular expansion of the Alfven waves/Poynting flux. The perpendicular expansion of the Alfven wave refers to either the perpendicular

propagation of the Alfven wave or the perpendicular expansion of the source region for generating the Alfven wave.

The auroral motion was 13.6 deg/min in the azimuthal direction. This is consistent with the typical value obtained in previous studies (Paschmann et al., 2003; Angelopoulos et al., 2008; Ogasawara et al., 2011). In addition, we observed a dipolarization with the azimuthal phase speed of 2 deg/min, which is consistent with the typical azimuthal speed of 30-50 km/s at geosynchronous orbit (Nagai, 1982; Ohtani et al., 2018). Therefore, in our event, the auroral motion is not directly linked to the dipolarization propagation. Instead, the auroral motion is directly linked to the perpendicular expansion of Alfven waves/Poynting flux, based on the correlation between the auroral brightness and Poynting flux at multiple locations during the auroral motion. Given the correlation between the aurora and Poynting flux, we infer that the perpendicular expansion of the Alfven wave/Poynting flux is also not directly linked to the dipolarization.

The azimuthal motion of the aurora has previously been linked to the azimuthal propagation of dipolarization (Angelopoulos et al., 2008; Ogasawara et al., 2011). These dipolarizations, which we refer to as the "fast" dipolarizations, are identified as B_z increase or B_x decrease on the order of several 10s sec. The "fast" dipolarizations would have a typical azimuthal speed around 150 km/s at geosynchronous orbit, which is much faster than the typical value of 30-50 km/s found in previous statistical studies (Nagai, 1982; Ohtani et al., 2018). Further investigation on all of the reported "fast" dipolarizations when both electric and magnetic field data are available shows that they are associated with Alfvenic Poynting fluxes (not shown). The period of the peak in the power of the Poynting flux ranges from ∼10-100 sec, equivalent to a frequency of 10-100 mHz in the spacecraft frame. The E/B ratio in this frequency range is on the order of local Alfven speed. All these features resemble the Poynting flux events in this and previous studies (Wygant et al., 2000; Dombeck et al., 2005; Keiling et al., 2003). Therefore, we propose that the signatures in B_x and B_z used for timing the previously reported "fast" dipolarizations can be explained as the signatures of Alfven waves in B_x and B_z. Consequently, the speed match between the auroral motion and fast" dipolarizations may effectively be explained as a direct correlation between the auroral brightening and Alfvenic Poynting flux during auroral motion, just as we have shown in this study.

Based on our observations, the dipolarization at 2 deg/min cannot be directly linked to the much faster auroral motion and the perpendicular expansion of Alfven waves. However, an indirect link may exist because dipolarizations are often observed around the time of the Poynting flux bursts, as in the event shown here and other events (Ergun et al., 2015). One potential explanation is the following coupling mechanism. The dipolarization and the associated flow may provide the free-energy source for generating Alfven waves. The Alfven wave growth rates are the largest around density gradients (e.g. the plasma sheet boundary layer) because velocity shear and phase shear are large (Lysak et al., 2009). In this scenario, during the slow (2 deg/min) and global (> 4 hours in MLT) azimuthal propagation of the dipolarization, there could be local generation and fast (> 10 deg/min) perpendicular expansion of Alfven waves near density gradients in the plasma sheet and its boundary layer. These Alfven waves are associated with earthward Poynting flux bursts which directly drive the auroral brightening and auroral motion.

5 Conclusions

Figure 6 summarizes the observations in the June 07, 2013 event. As shown in Section 3, a dipolarization was seen to propagate from 0 MLT to 20 MLT during 25 min. The westward phase speed of the dipolarization was 2 deg/min, which translates

to about 20 km/s at 5 Re. Around the time when the dipolarization passed the RBSP satellites, intense earthward Alfvenic Poynting flux was observed at both satellites and westward auroral motion of 13.6 deg/min was observed in the ionosphere. A temporal and spatial correlation was found between the Poynting flux and the auroral brightness at the spacecraft footpoint, suggesting that the Alfvenic Poynting flux powers the auroral acceleration and that the Alfven waves couple the auroral acceleration region to the near-earth plasma sheet boundary layer (PSBL).

These observations offer strong evidence for Alfven waves as the primary driver of auroral acceleration during a substorm. The results also suggest that the dipolarization was not directly involved in the coupling between the auroral and PSBL. However, dipolarizations have long been known to play a key role during geomagnetic substorms (e.g. Fu et al., 2020, and references therein). For example, our study suggests that the dipolarization may be related to the generation of the observed Alfvenic Poynting flux. The relationship between dipolarizations and Alfven waves/Poynting flux is important for understanding the major energy conversions during geomagnetic substorms, and further study is necessary to acquire a complete picture of the substorm driving process.

Acknowledgments

The authors thank the Van Allen Probes teams, especially the HOPE and EMFISIS teams, for their support. This work was supported at UMN by the NASA grant 80NSSC19K0306 and by the contract from JHU/APL under NASA prime contract NAS5-01072. HOPE data are available from the RBSP-ECT SOC at `https://rbsp-ect.newmexicoconsortium.org/rbsp_ect.php`. EFW and EMFISIS data are available at `https://cdaweb.gsfc.nasa.gov/pub/data/rbsp`. THEMIS all-sky imager data are available at `http://themis.ssl.berkeley.edu/data/themis/thg/l1/asi/`.

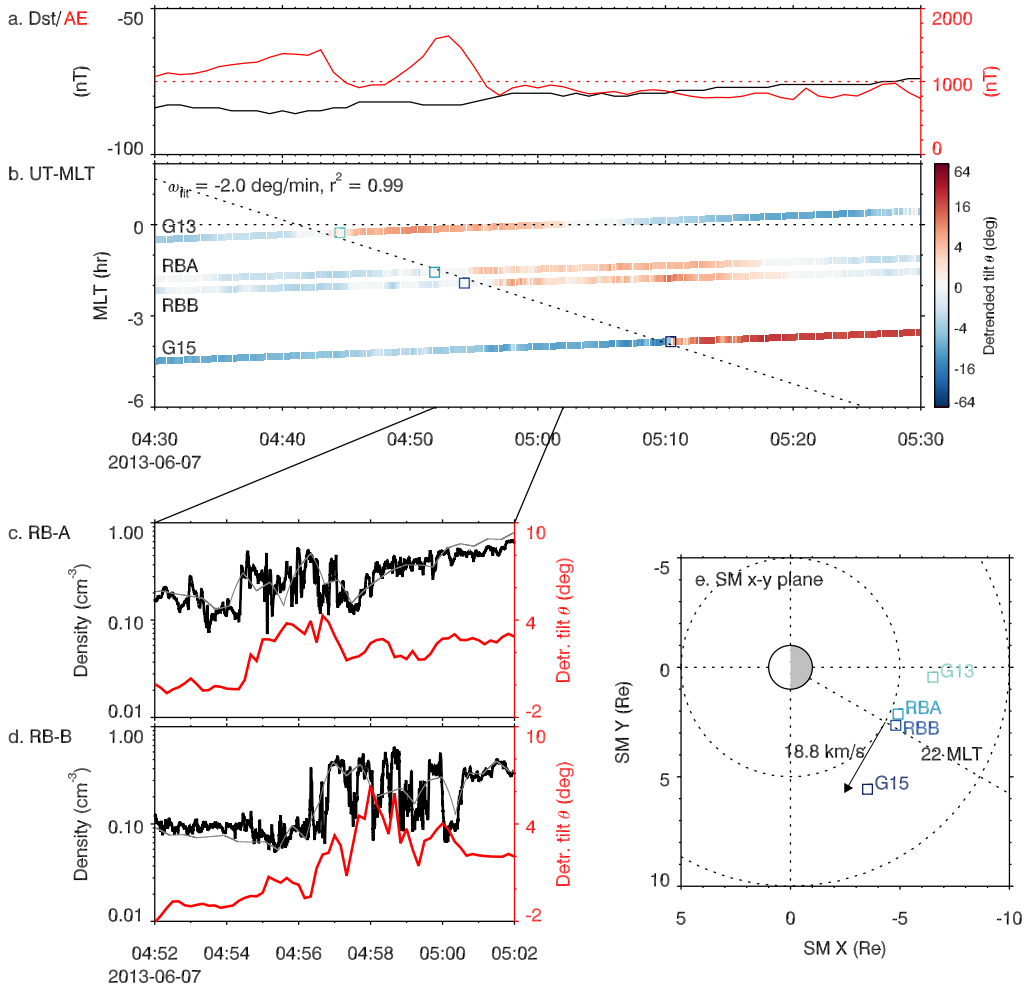

Figure 1. The dipolarization propagated westward with density structures during a substorm on June 07, 2013. Panel a shows the Dst and AE indices, showing a substorm around 04:47 to 04:57 UT during the recovery phase of a storm. Panel b shows the dipolarization as measured in tilt angle color-coded along tracks of 4 spacecraft (GOES-13 and -15 and RBSP-A and -B) in the pre-midnight section. At each satellite, the time of dipolarization is when the increasing tilt angle crosses 0 (where blue turns red). A linear fit on the times and MLTs of the dipolarization determines the drift of dipolarization in MLT to be 2 deg/min. Panel c and d show the density as determined from the particle instrument (low-resolution, gray) and spacecraft potential (high-resolution, black), and the detrended tilt angle (red). Panel e shows the azimuthal phase speed of the dipolarization scaled to the spacecraft location.

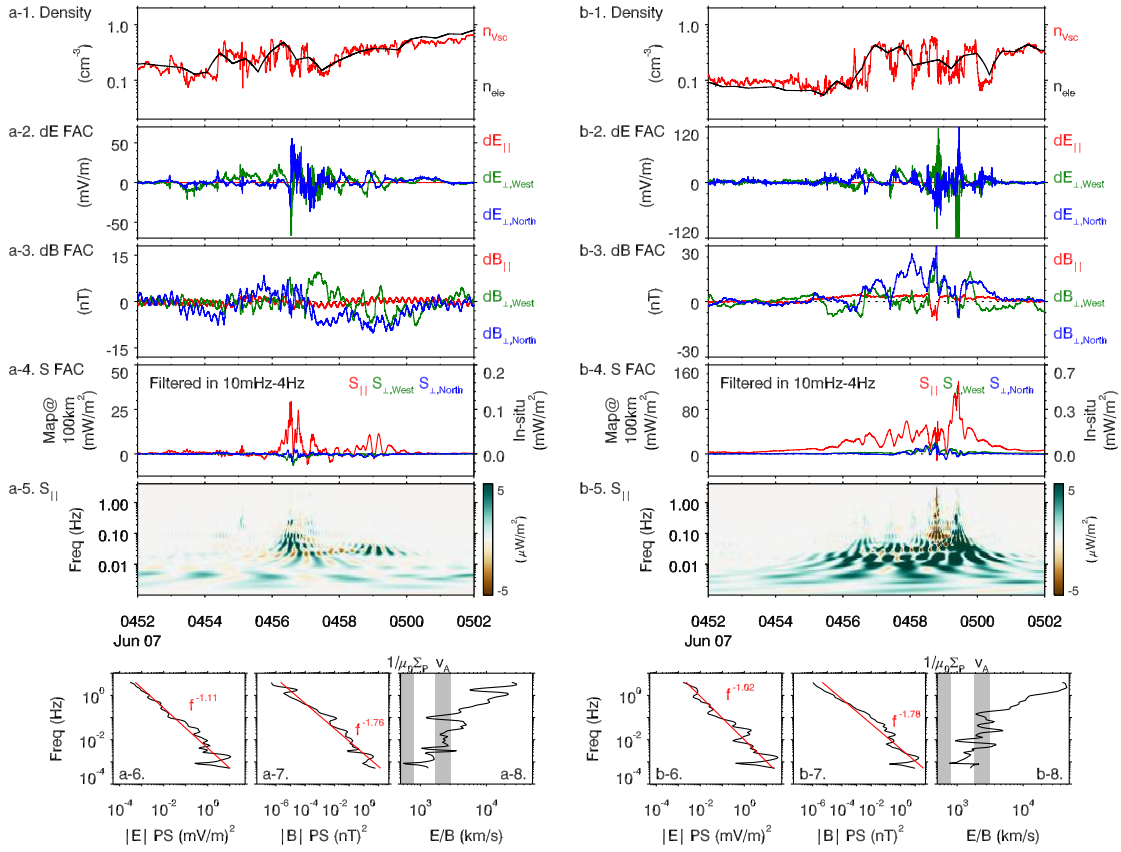

Figure 2. Poynting flux calculation and properties. Data for RBSP-A are presented in the panels on the left and RBSP-B data are on the right in the same format. Panel a-1 shows the same density data in Figure 1c for reference purposes. Panel a-2 and a-3 show the waveforms of the wave electric and magnetic fields in the field-aligned coordinate (FAC), where the components are parallel (red), westward (green) and northward (blue). Panel a-4 shows the Poynting flux filtered in 10 mHz to 4 Hz before and after normalized to 100 km to account for the converging flux tube. Panel a-5 shows the parallel component of the Poynting flux in the time-frequency domain before integration. Panel a-6 and a-7 show the power spectra of the electric and magnetic field. Panel a-8 shows the E/B ratio as a function of frequency. The shaded areas are the E/B ratios expected for the Pedersen conductivity and Alfven waves, where v_A is calculated from the measured magnetic field, density and ion species. The Poynting fluxes at both spacecraft were predominantly earthward. The main power ranged 10-100 mHz and in this range the E/B ratio is comparable to the local Alfven speed.

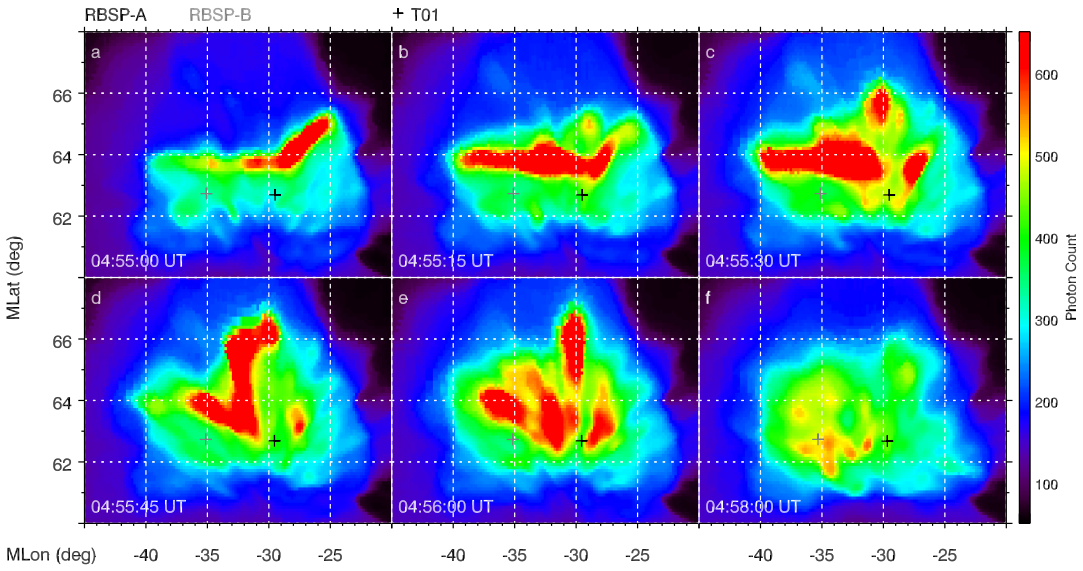

Figure 3. Snapshots of the auroral westward (panels a and b) and poleward (panels b to d) motions and the feinting of the auroral activity (panels e to f) from the Movie S1 of the supporting information. The footprints of RBSP-A (black) and -B (gray) are over-plotted.

References

Akasofu, S.-I. (1964). The development of the auroral substorm. *Planetary and Space Science*, *12*(4), 273 – 282. Retrieved from `http://www.sciencedirect.com/science/article/pii/0032063364901515` doi: http://dx.doi.org/10.1016/0032-0633(64)90151-5

Angelopoulos, V., Baumjohann, W., Kennel, C. F., Coroniti, F. V., Kivelson, M. G., Pellat, R., ... Paschmann, G. (1992). Bursty bulk flows in the inner central plasma sheet. *Journal of Geophysical Research: Space Physics*, *97*(A4), 4027–4039. Retrieved from `http://dx.doi.org/10.1029/91JA02701` doi: 10.1029/91JA02701

Angelopoulos, V., Sibeck, D., Carlson, C. W., McFadden, J. P., Larson, D., Lin, R. P., ... Sigwarth, J. (2008, dec). First Results from the THEMIS Mission. *Space Science Reviews*, *141*(1), 453–476. Retrieved from `https://doi.org/10.1007/s11214-008-9378-4` doi: 10.1007/s11214-008-9378-4

Chaston, C. C., Bonnell, J. W., Carlson, C. W., McFadden, J. P., Ergun, R. E., Strangeway, R. J., & Lund, E. J. (2004). Auroral ion acceleration in dispersive Alfvén waves. *Journal of Geophysical Research: Space Physics*, *109*(A4), n/a–n/a. Retrieved from `http://dx.doi.org/10.1029/2003JA010053` doi: 10.1029/2003JA010053

Dombeck, J., Cattell, C. A., Wygant, J. R., Keiling, A., & Scudder, J. (2005, dec). Alfvén waves and Poynting flux observed simultaneously by Polar and FAST in the plasma sheet boundary layer. *J. Geophys. Res.*, *110*(A12), A12S90. Retrieved from `http://dx.doi.org/10.1029/2005JA011269` doi: 10.1029/2005JA011269

Ergun, R. E., Goodrich, K. A., Stawarz, J. E., Andersson, L., & Angelopoulos, V. (2015). Large-amplitude electric fields associated with bursty bulk flow braking in the Earth's plasma sheet. *Journal of Geophysical Research: Space Physics*, *120*(3), 1832–1844. Retrieved from `http://dx.doi.org/10.1002/`

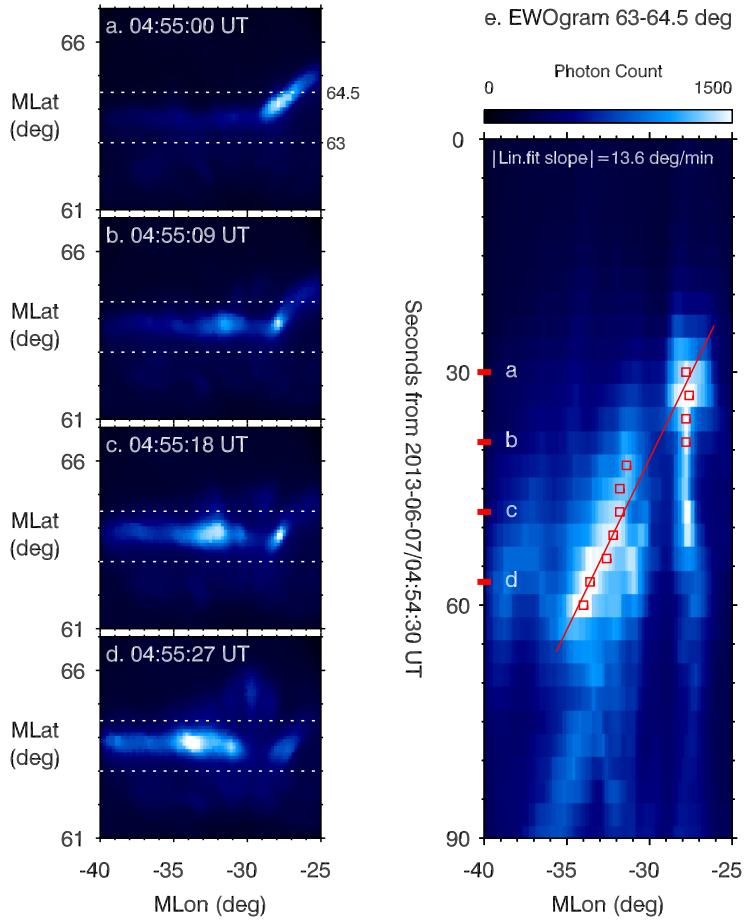

Figure 4. Determining the westward motion through the EWOgram between 63-64.5 deg MLat. The westward motion is 13.6 deg/min, determined through a linear fit of the MLon of the brightest aurora in each time frame. This speed is about 6 times of the westward speed of the dipolarization. The region around -30 deg MLon could be either a ground object blocking the camera or a physical dark region of the aurora. Because of the ambiguity, the four red boxes around the dark region are not used for the linear fit (including them results in a similar value of 14.3 deg/min).

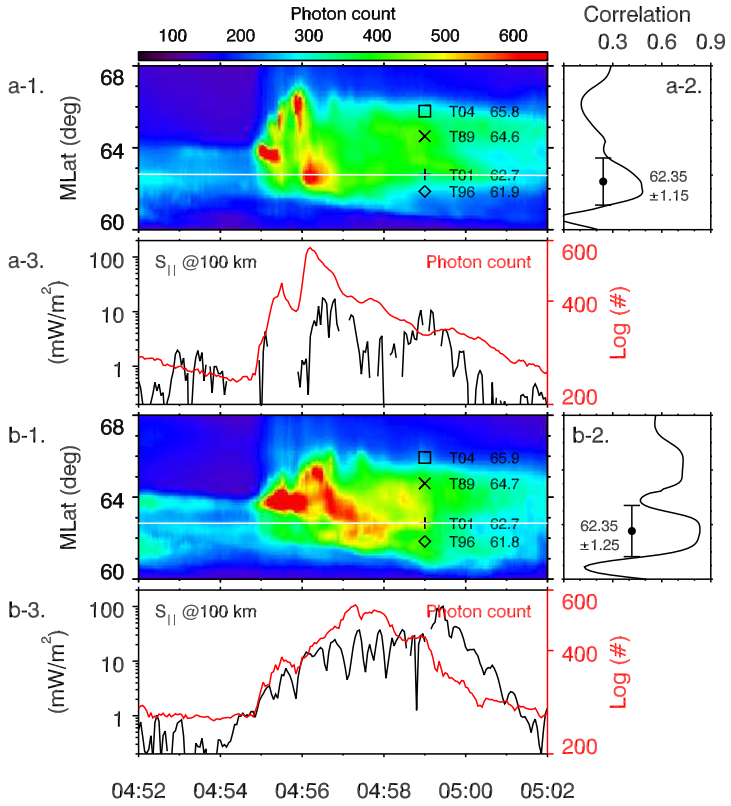

Figure 5. The spatial and temporal correlation between the Poynting flux and the auroral brightness around the footpoint. Panel a-1 shows the auroral KEOgram around the MLon of RBSP-A. The MLat of the footpoint according to 4 Tsyganenko models are over plotted. Although a wide range of MLat is predicted, the T01 model is chosen for two reasons. Firstly, T01 predicted the in-situ magnetic field the best. Secondly, as shown in panel a-2, cross-correlation between the Poynting flux and the auroral brightness at all MLat peaks around the T01 MLat. The T01 MLat is marked by the white line in panel a-1. For the same reason, panel b1- to b-2 show that the T01 model also works for RBSP-B. Panel a-3 and b-3 show the Poynting flux and the auroral brightness at the T01 MLat. After 04:58 UT the correlation weakens somewhat, consistent with the fact that the satellite is moving out of the field of view of the auroral imager.

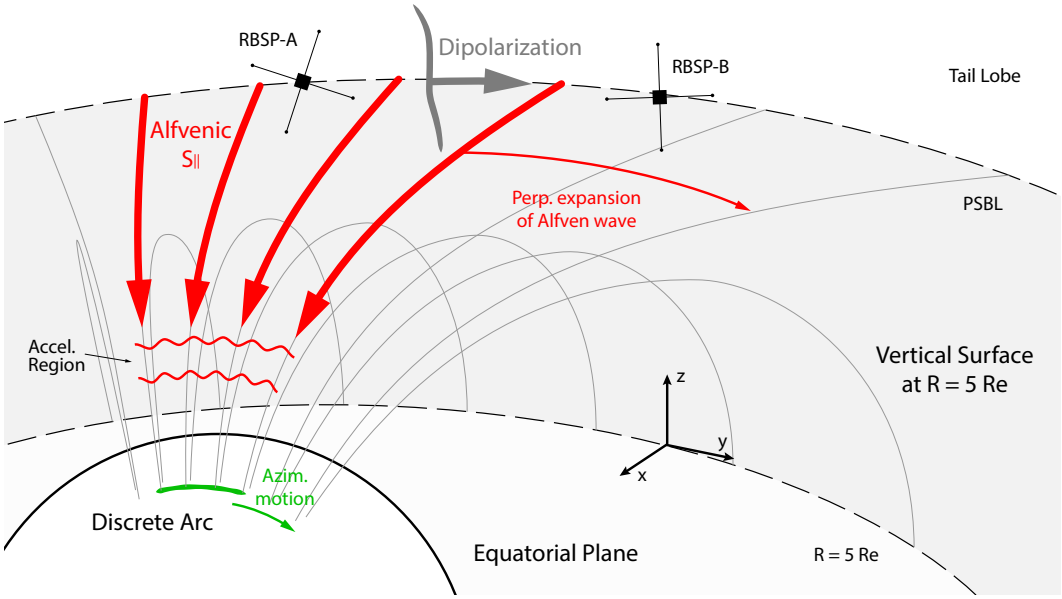

Figure 6. A schematic view to summarize the observations between the auroral ionosphere and the inner-magnetosphere. The curved gray wall is a vertical cylindrical surface at 5 Re, containing the two RBSP spacecraft. The earthward Alfvenic Poynting flux transmits electromagnetic energy to the ionosphere, while auroral brightening and a dipolarization are co-observed. A possible chain of energy conversion includes: Poynting flux (shear Alfven wave) is generated related to the dipolarization; The Alfven waves propagate earthward to transmit the electromagnetic energy to lower altitude, powering the parallel acceleration of electrons around the auroral acceleration region. The westward motion of the aurora is directly linked to the perpendicular expansion of Alfven waves.

2014JA020165 doi: 10.1002/2014JA020165

Fu, H., Grigorenko, E. E., Gabrielse, C., Liu, C., Lu, S., Hwang, K. J., ... Chen, F. (2020). Magnetotail dipolarization fronts and particle acceleration: A review. *Science China Earth Sciences*, *63*(2), 235–256. Retrieved from https://doi.org/10.1007/s11430-019-9551-y doi: 10.1007/s11430-019-9551-y

Funsten, H. O., Skoug, R. M., Guthrie, A. A., MacDonald, E. A., Baldonado, J. R., Harper, R. W., ... Chen, J. (2013). Helium, Oxygen, Proton, and Electron (HOPE) Mass Spectrometer for the Radiation Belt Storm Probes Mission. *Space Science Reviews*, 1–62. Retrieved from http://dx.doi.org/10.1007/s11214-013-9968-7 doi: 10.1007/s11214-013-9968-7

Keiling, A., Wygant, J. R., Cattell, C. A., Mozer, F. S., & Russell, C. T. (2003, jan). The Global Morphology of Wave Poynting Flux: Powering the Aurora. *Science*, *299*(5605), 383 –386. Retrieved from http://www.sciencemag.org/content/299/5605/383.abstract doi: 10.1126/science.1080073

Kletzing, C. A., Kurth, W. S., Acuna, M., MacDowall, R. J., Torbert, R. B., Averkamp, T., ... Tyler, J. (2013, nov). The Electric and Magnetic Field Instrument Suite and Integrated Science (EMFISIS) on RBSP. *Space Science Reviews*, *179*(1), 127–181. Retrieved from https://doi.org/10.1007/s11214-013-9993-6 doi: 10.1007/s11214-013-9993-6

Lysak, R. L., Song, Y., & Jones, T. W. (2009). Propagation of Alfvén waves in the magnetotail during substorms. *Annales Geophysicae*, *27*(5), 2237–2246. Retrieved from http://www.ann-geophys.net/27/2237/2009/ doi: 10.5194/angeo-27-2237-2009

McFadden, J. P., Carlson, C. W., & Ergun, R. E. (1999). Microstructure of the auroral acceleration region as observed by FAST. *Journal of Geophysical Research: Space Physics*, *104*(A7), 14453–14480. Retrieved from http://dx.doi.org/10.1029/1998JA900167 doi: 10.1029/1998JA900167

Mende, S. B., Harris, S. E., Frey, H. U., Angelopoulos, V., Russell, C. T., Donovan, E., ... Peticolas, L. M. (2008, jun). The THEMIS Array of Ground-based Observatories for the Study of Auroral Substorms. *Space Science Reviews*, *141*(1), 357. Retrieved from https://doi.org/10.1007/s11214-008-9380-x doi: 10.1007/s11214-008-9380-x

Nagai, T. (1982). Observed magnetic substorm signatures at synchronous altitude. *Journal of Geophysical Research: Space Physics*, *87*(A6), 4405–4417. Retrieved from https://agupubs.onlinelibrary.wiley.com/doi/abs/10.1029/JA087iA06p04405 doi: 10.1029/JA087iA06p04405

Ogasawara, K., Kasaba, Y., Nishimura, Y., Hori, T., Takada, T., Miyashita, Y., ... Bonnell, J. (2011). Azimuthal auroral expansion associated with fast flows in the near-Earth plasma sheet: Coordinated observations of the THEMIS all-sky imagers and multiple spacecraft. *Journal of Geophysical Research: Space Physics*, *116*(A6). Retrieved from https://agupubs.onlinelibrary.wiley.com/doi/abs/10.1029/2010JA016032 doi: 10.1029/2010JA016032

Ohtani, S., Motoba, T., Gkioulidou, M., Takahashi, K., & Singer, H. J. (2018). Spatial Development of the Dipolarization Region in the Inner Magnetosphere. *Journal of Geophysical Research: Space Physics*, *123*(7), 5452–5463. Retrieved from https://agupubs.onlinelibrary.wiley.com/doi/abs/10.1029/2018JA025443 doi: 10.1029/2018JA025443

Paschmann, G., Håland, S., & Treumann, R. (2003). *Auroral Plasma Physics*. Kluwer Academic Pub. Retrieved from http://books.google.com/books?id=xYFjIrDlGqIC

Runov, A., Angelopoulos, V., Sitnov, M. I., Sergeev, V. A., Bonnell, J., McFadden, J. P., ... Auster, U. (2009). THEMIS observations of an earthward-propagating dipolarization front. *Geophysical Research Letters*, *36*(14). Retrieved from http://dx.doi.org/10.1029/2009GL038980 doi: 10.1029/

2009GL038980

Spence, H. E., Reeves, G. D., Baker, D. N., Blake, J. B., Bolton, M., Bourdarie, S., ... Thorne, R. M. (2013). Science Goals and Overview of the Radiation Belt Storm Probes (RBSP) Energetic Particle, Composition, and Thermal Plasma (ECT) Suite on NASA's Van Allen Probes Mission. *Space Science Reviews*, *179*(1), 311–336. Retrieved from https://doi.org/10.1007/s11214-013-0007-5 doi: 10.1007/s11214-013-0007-5

Tsyganenko, N. (1996, oct). Effects of the solar wind conditions in the global magnetospheric configurations as deduced from data-based field models (Invited). In E. Rolfe & B. Kaldeich (Eds.), *International conference on substorms* (Vol. 389, p. 181).

Tsyganenko, N. A. (1989). A magnetospheric magnetic field model with a warped tail current sheet. *Planetary and Space Science*, *37*(1), 5–20. Retrieved from http://www.sciencedirect.com/science/article/pii/0032063389900664 doi: http://dx.doi.org/10.1016/0032-0633(89)90066-4

Tsyganenko, N. A. (2002). A model of the near magnetosphere with a dawn-dusk asymmetry 2. Parameterization and fitting to observations. *Journal of Geophysical Research: Space Physics*, *107*(A8), SMP 10–1—-SMP 10–17. Retrieved from http://dx.doi.org/10.1029/2001JA000220 doi: 10.1029/2001JA000220

Tsyganenko, N. A., & Sitnov, M. I. (2005). Modeling the dynamics of the inner magnetosphere during strong geomagnetic storms. *Journal of Geophysical Research: Space Physics*, *110*(A3), n/a—-n/a. Retrieved from http://dx.doi.org/10.1029/2004JA010798 doi: 10.1029/2004JA010798

Wygant, J. R., Bonnell, J. W., Goetz, K., Ergun, R. E., Mozer, F. S., Bale, S. D., ... Tao, J. B. (2013, nov). The Electric Field and Waves Instruments on the Radiation Belt Storm Probes Mission. *Space Science Reviews*, *179*(1), 183–220. Retrieved from https://doi.org/10.1007/s11214-013-0013-7 doi: 10.1007/s11214-013-0013-7

Wygant, J. R., Keiling, A., Cattell, C. A., Johnson, M., Lysak, R. L., Temerin, M., ... Spann, J. (2000). Polar spacecraft based comparisons of intense electric fields and Poynting flux near and within the plasma sheet-tail lobe boundary to UVI images: An energy source for the aurora. *J. Geophys. Res.*, *105*(A8), 18675–18692. Retrieved from http://dx.doi.org/10.1029/1999JA900500 doi: 10.1029/1999JA900500

Wygant, J. R., Keiling, A., Cattell, C. A., Lysak, R. L., Temerin, M., Mozer, F. S., ... Russell, C. T. (2002). Evidence for kinetic Alfvén waves and parallel electron energization at 4-6 RE altitudes in the plasma sheet boundary layer. *J. Geophys. Res.*, *107*(A8), 1201. Retrieved from http://dx.doi.org/10.1029/2001JA900113 doi: 10.1029/2001JA900113

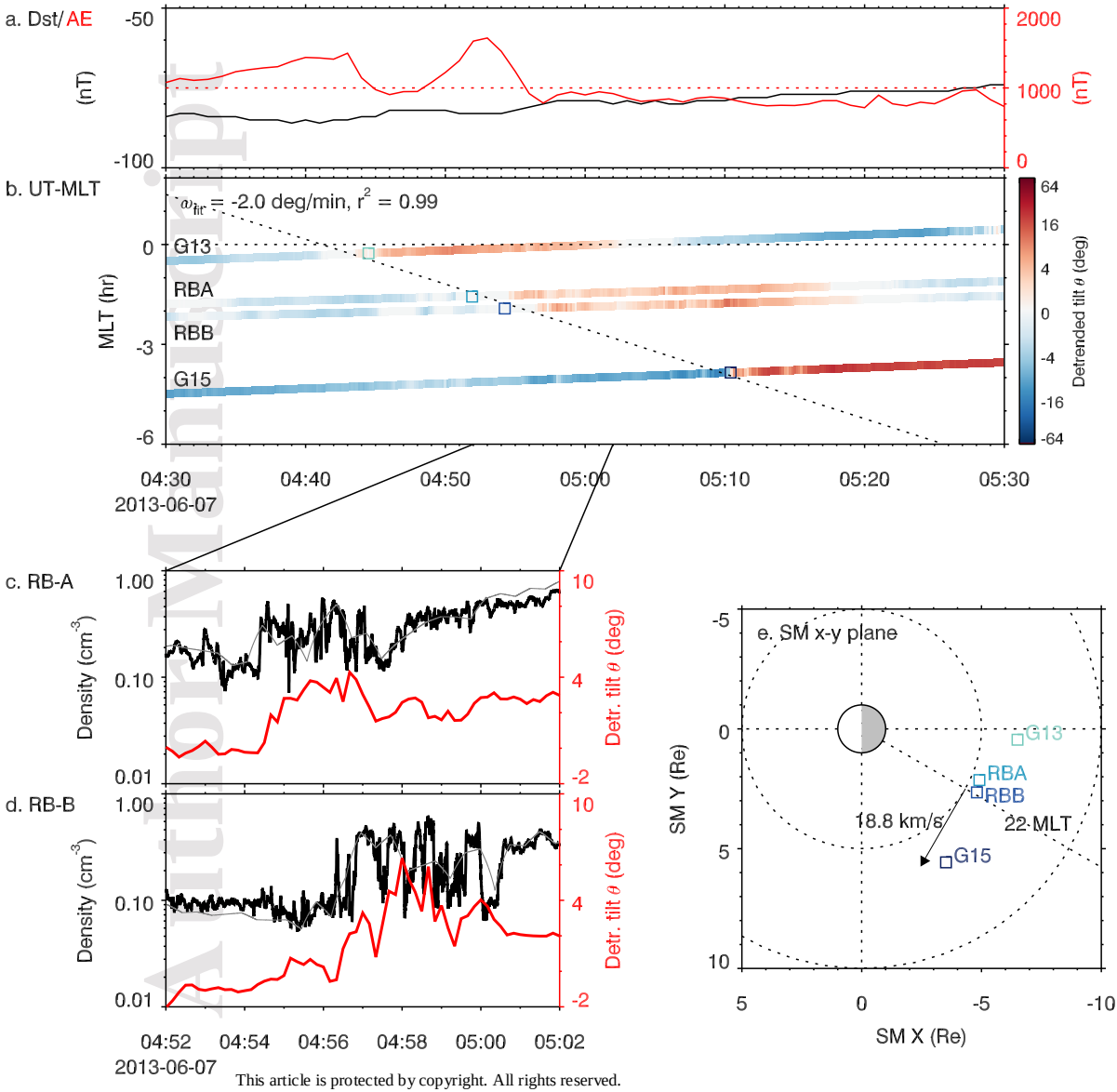

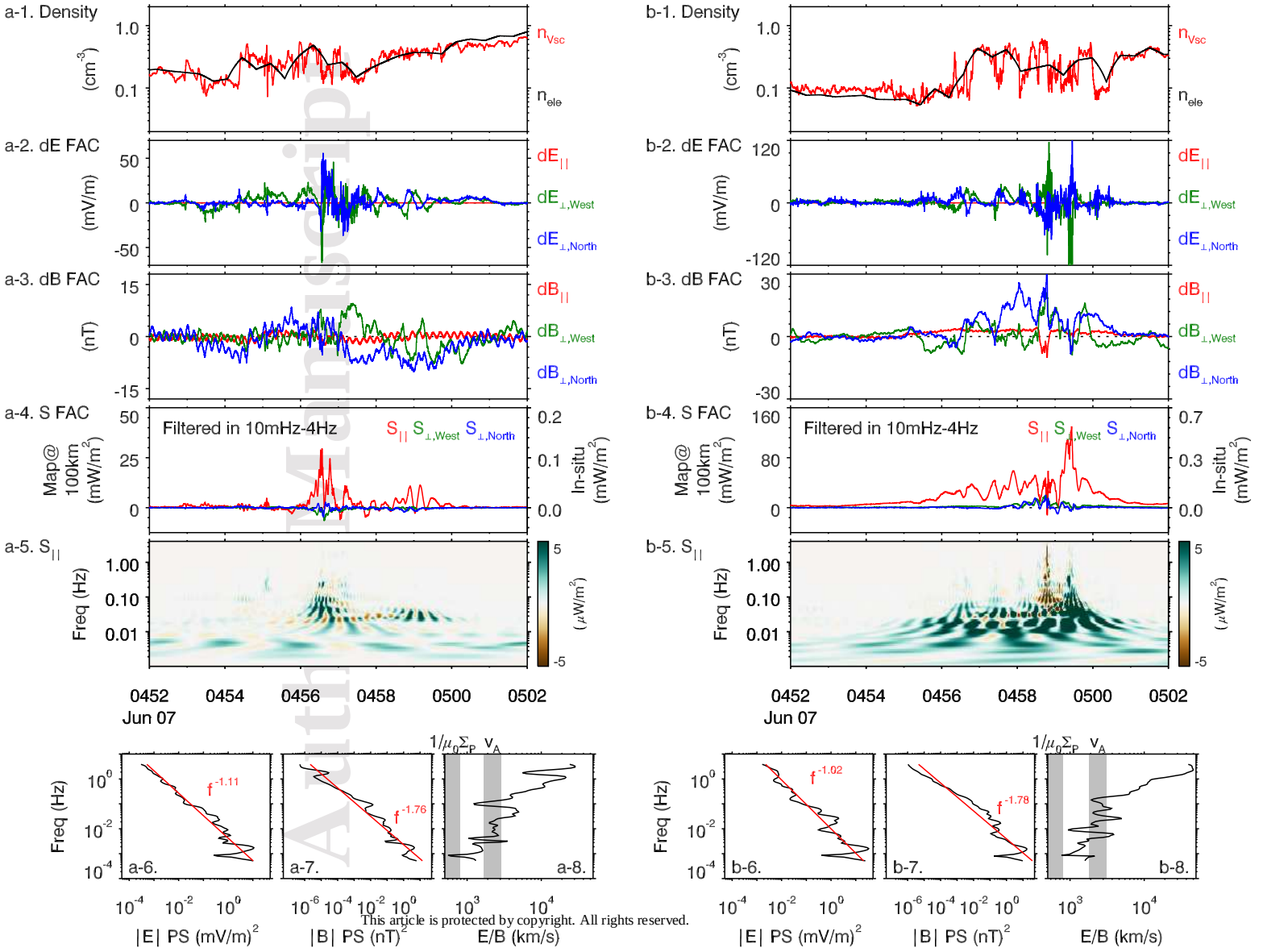

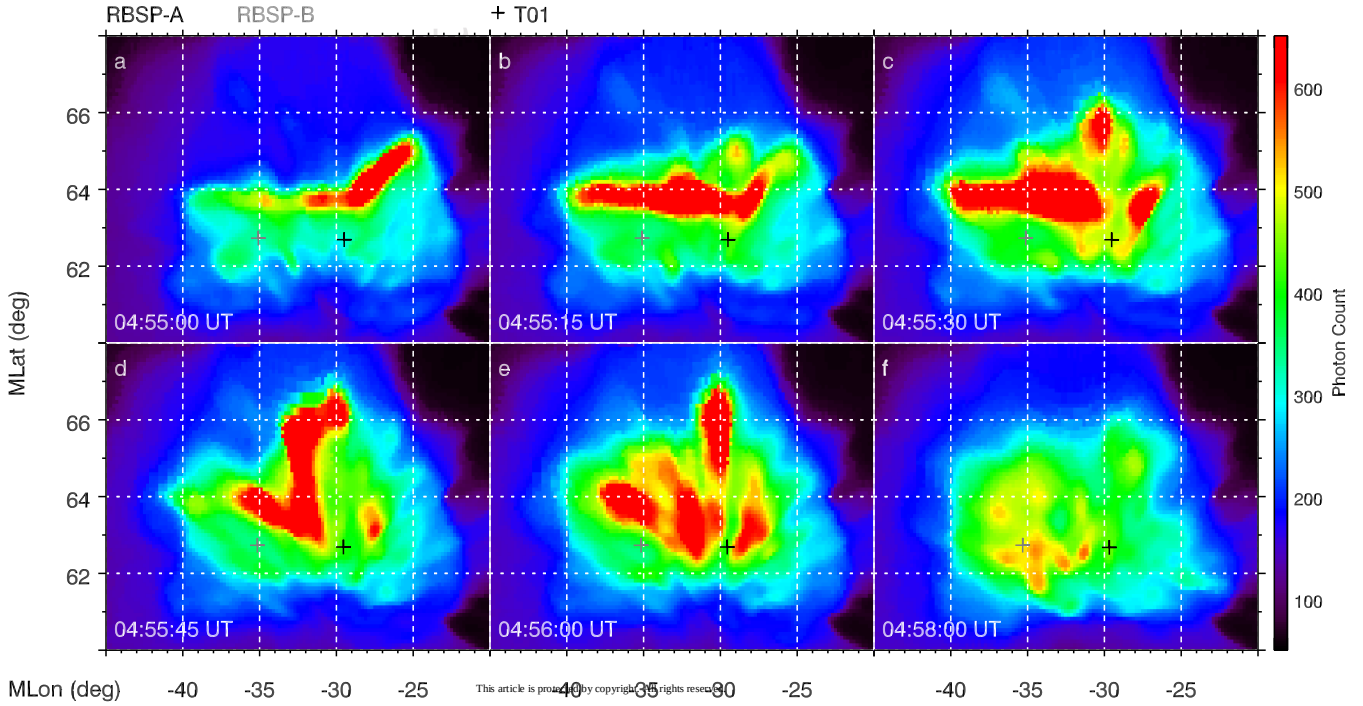

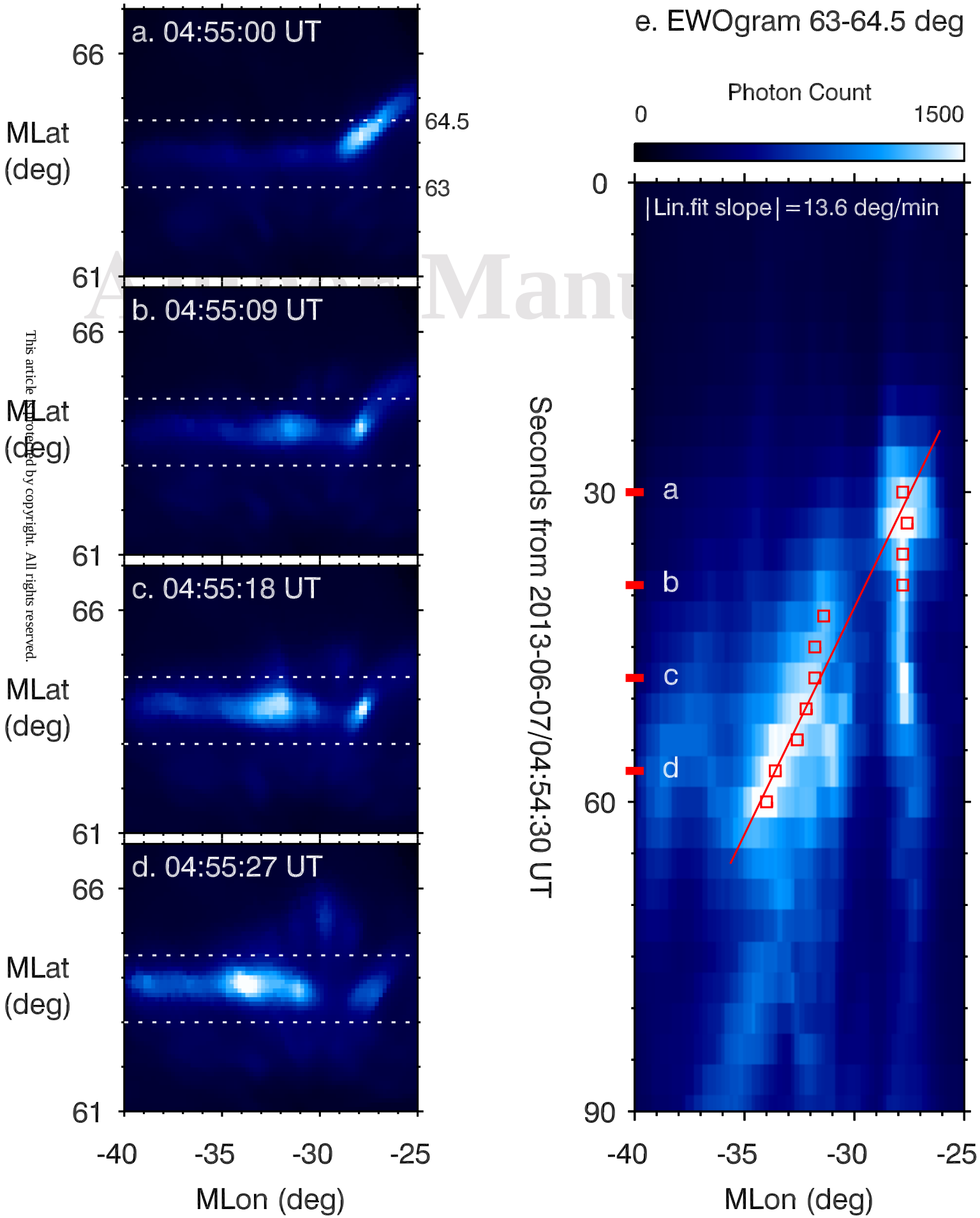

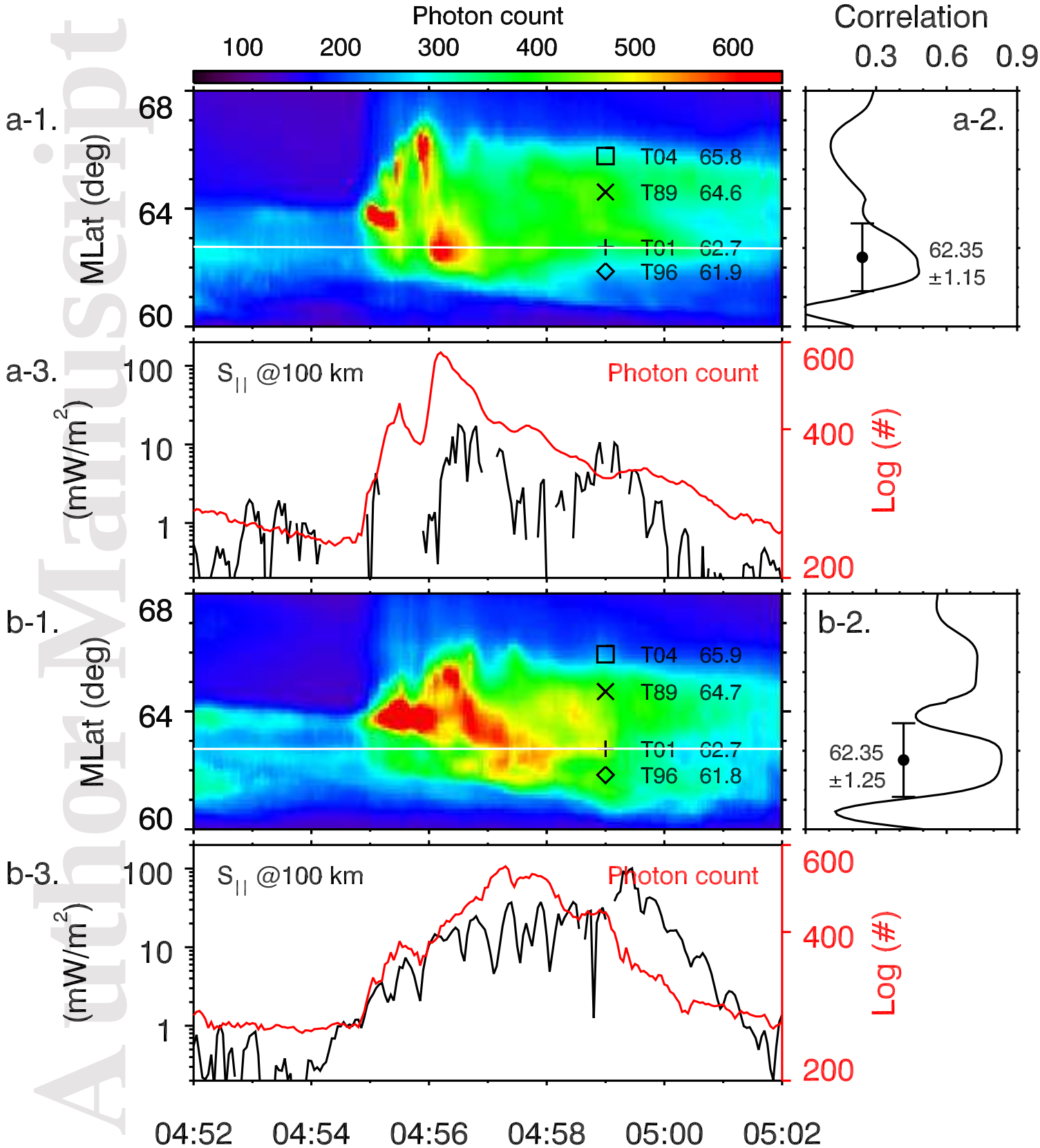

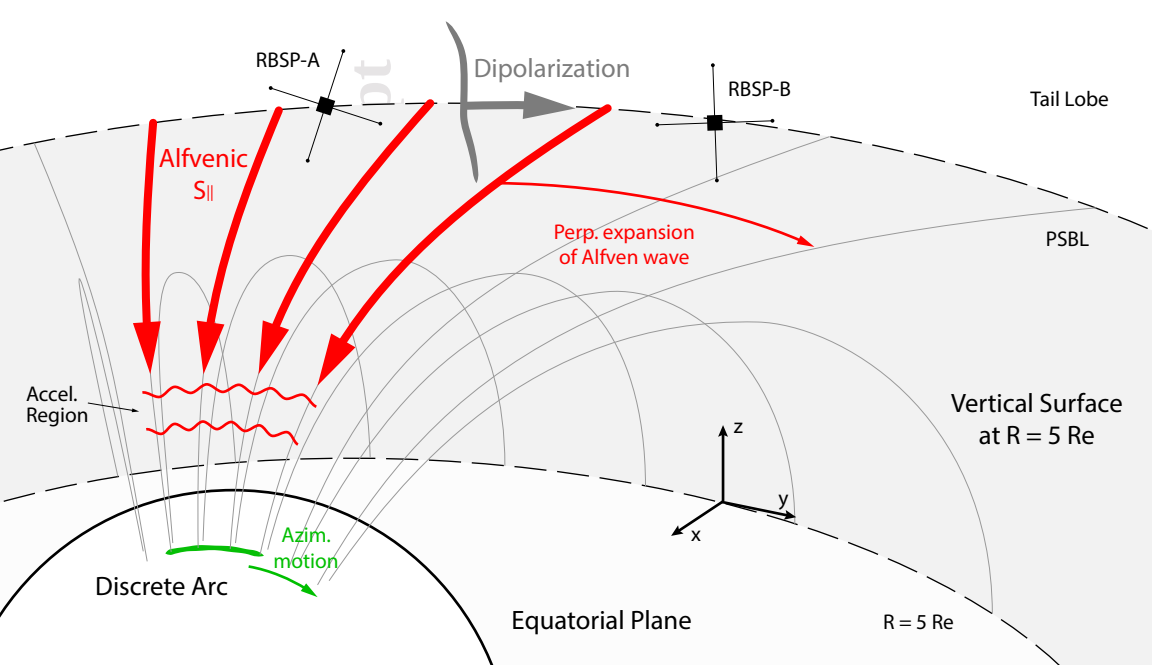
RBSP-A
Dipolarization
RBSP-B
Tail Lobe
Alfvenic
S||
Perp. expansion
of Alfven wave
PSBL
Accel.
Region
Vertical Surface
at R = 5 Re
z
y
x
Azim.
motion
Discrete Arc
Equatorial Plane
R = 5 Re